Raman Investigation of the N_2-O_2 Binary System as a Function of Pressure and Temperature

Maksym Minenko,[†] Jörg Kreutz,*[,†] Thorsten Hupprich,[†,‡] and Hans-Jörg Jodl[†,§]

University of Kaiserslautern, Department of Physics, Erwin Schrödinger Strasse, 67663 Kaiserslautern, Germany, and LENS, European Laboratory for Non Linear Spectroscopy, 50019 Sesto-Fiorentino, Florence, Italy

Received: September 5, 2003; In Final Form: March 16, 2004

We produced mixtures of N_2-O_2 with different concentrations and performed low-temperature Raman studies at ambient and high pressures. From spectra in vibron and phonon regions, we determined band frequency, bandwidth, and band intensity as a function of temperature, pressure, and concentration. We determined the vibron Raman cross-sections and deduced the true concentrations of mixtures from vibron Raman band intensities. These concentrations were different from those determined from partial gas pressure of the initial gaseous mixtures. From fingerprints in Raman spectra, such as jumps in band frequencies or additional band splitting, we were able to prove phase transitions and propose a preliminary $T-x$ phase diagram. We compared this diagram with two reported in the literature from structural analysis. Comparing all three variants of the $T-x$ phase diagrams we found several discrepancies and inconsistencies, which we associate with different solid sample production techniques. Since we could prove that our samples were in thermodynamic equilibrium, we are convinced that we improved the known phase diagram substantially. From Raman band intensities of the O_2 vibrations in different phases of N_2 and O_2, we were able to determine quantitatively the solubility of O_2 in N_2. Preliminary Raman studies of 2% and 7% O_2 in N_2 at high pressure and low temperatures showed that a larger amount of O_2 can be dissolved in N_2 than at ambient pressure. At the critical pressure ($p \sim 15$ GPa) we found from Raman spectra that O_2 is demixed from 7% O_2 in N_2 to form ϵ-O_2. This was previously called a "new phase" in the literature and not understood up to now. Finally, from band frequencies we determined the environmental shift of oxygen molecules in the mixture which is related to the intermolecular potential $U(N_2-O_2)$ between different types of molecules.

1. Introduction

van der Waals crystals such as rare gas solids (RGS) or molecular crystals N_2, O_2, CO, CO_2, and their mixtures have been studied extensively since 1950 in various contexts: molecular solids as matrix materials,[1] modeling of astrophysical data,[2] simulation of solid state and thermodynamic results by molecular dynamics or Monte Carlo methods,[3] and the application of ultra high-pressure (Mbar regime).[4] Although pure molecular crystals are quite well studied,[5] their mixtures are still far from being understood. Results in the literature suffer very often from discrepancies or unreproduced data.

Since N_2 is the molecular crystal par excellence, initial investigations were of mixed molecular crystals with the system N_2 + x (x = RGS, CO, O_2).[6−10] In α-N_2 the electrostatic quadrupole−quadrupole interaction is dominant. This type of interaction can be systematically tuned by doping with Ar-atoms. Knorr et al.[11] reported in a series of papers on the orientational glass of Ar-doped N_2 by structural and infrared spectroscopic techniques. Since Ar is neither Raman- nor IR-active, one can probe the behavior of the mixture only by means of N_2-modes (vibron, phonons). Since N_2 and CO are isomorphous and isoelectronic, their mixing parameters are ideal for the study of mixtures. However, CO spectra (Raman, IR-absorption) are very broad due to strong anharmonicities and mode coupling. Therefore, we chose the less studied N_2-O_2 system for our investigations.

We will briefly summarize relevant literature on this mixture at ambient pressure. Reference 12 gives an overview of structural and thermophysical properties of N_2-O_2 mixtures (up to about 1996). Ruheman et al.[13] constructed the liquid−solid phase diagram on the basis of calorimetric measurements. Standard X-ray techniques were used by two groups[14,15] to study the structure of solid phases and to construct a $T-x$ diagram for N_2-O_2 with many inconsistencies. Both phase diagrams (see Figure 1) are similar with respect to regions of phases and temperatures for phase transitions. Barrett et al.[14] examined the solubility of O_2 in N_2 at low temperatures and found it to be strongly temperature-dependent (from 10% to 0%), whereas Baryl'nik et al.[15] found that this solubility is almost constant at ∼18%. An additional metastable x-phase (see Figure 1) was always present in the studies by Barrett et al. and present but avoidable in those of Baryl'nik et al. Minor differences in some regions exist in both studies between 30 and 50 K. The influence of sample production and preparation must be considered as well. Barrett et al. cooled the liquid rapidly, whereas Baryl'nik et al. condensed the gas on a substrate at low temperature. In contrast, we cooled our actual sample from liquid slowly over days or weeks.

Besides structural analysis, only one spectroscopic and one theoretical investigation were reported at ambient pressure.

* Author to whom correspondence should be addressed. E-mail: kreutz@physik.uni-kl.de.
† University of Kaiserslautern.
‡ Present address: Albanusstrasse 13, 55128 Mainz, Germany.
§ LENS.

10.1021/jp036658r CCC: $27.50
Published on Web 04/27/2004

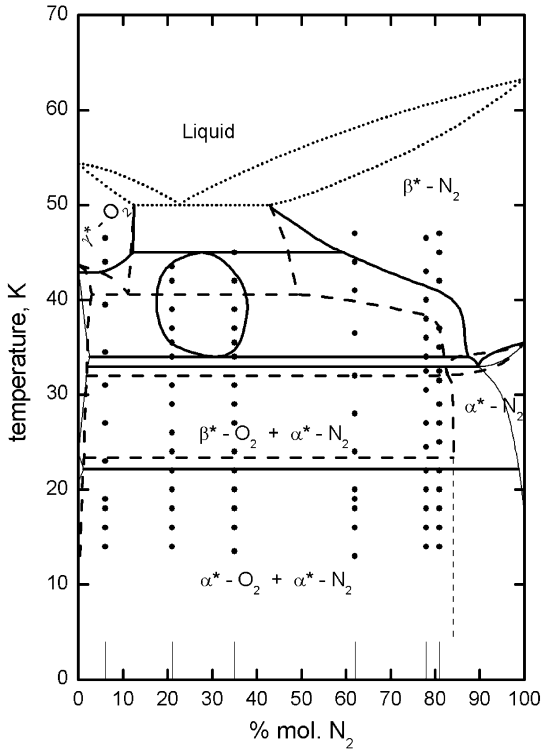

Figure 1. $T-$concentration phase diagram of N_2-O_2 from structural analyses reported by two different groups: solid lines—Barrett et al.,[14] broken lines—Baryl'nik et al.[15] Thin lines are only assumptions of aforementioned authors. Thick points represent our measurements at different temperatures at a given concentration. The transition from liquid to solid (dotted lines) was studied by Ruheman et al.[13] Phase designation is indicated within the ranges where the description is clear. The encircled area in the diagram of Barrett et al. indicates a metastable phase region.

Pritula and Khashchina[16] performed FTIR studies on the nitrogen−oxygen binary mixed system in the far IR and measured the O_2-magnon frequency as a function of the N_2 concentration. Freiman et al.[17] presented theoretical studies of magnetic properties of oxygen pair clusters for different geometries that can be realized in the N_2-O_2 binary mixed system. These authors predicted anomalous temperature and pressure behavior of the magnetic susceptibility, heat capacity, and entropy.

Only two groups investigated the N_2-O_2 solid mixtures under pressure. Baer and Nicol[18] applied high-pressure to the mixed system to determine indirectly parts of the $p-x$ diagram by Raman scattering at $T = 300$ K, measuring the N_2 or O_2 vibron and libron frequencies $\omega(p, x)$. At pressures higher than 11 GPa they found that oxygen and nitrogen molecules form a new solid phase. Although many aspects are unclear or open, it is a study which should be extended to low temperatures. Damde and Jodl[19] performed Raman measurements at 18 K and pressures up to 25 GPa for several N_2-O_2 mixtures. Following the idea of Feile et al.[9a] for the N_2-Ar system, the authors also analyzed the concentration-dependent intensity ratio of the nitrogen peaks; it appeared that the dopant O_2 molecules were not preferentially embedded on c-sites (symmetry S_6) of ϵ*-N_2 as is the case of N_2-Ar. Damde and Jodl[19] also measured the spectral features of the "new phase" at low temperatures. As in ref 18, no explanation for this phase was given.

The essence of these studies during the past decades is that the N_2-O_2 mixed system is very interesting with respect to solubility, miscibility, metastability, order/disorder phenomena, different trapping sites, simulation studies, and phase transition kinetics—but is far from understood. The contradictions or discrepancies in the ambient pressure literature might be due to different sample production, different preparation of mixtures, sample treatment, unknown sensitivity to impurities, etc. Traditionally, X-ray structural analysis or calorimetry is used to establish phase diagrams. We propose to use optical spectroscopy combined with group theory as a complementary technique. From fingerprints in optical spectra of all elementary excitations (phonons, vibrons), we are able to deduce phase transitions in the $p-T-x$ diagram. Therefore, we investigated the N_2-O_2 system (nine concentrations) by Raman scattering in a series of experiments at ambient and at high pressure, as well as at room and low temperatures.

The aim of this publication is to study samples in thermodynamic equilibrium by means of Raman spectroscopy in order to answer some open areas which appeared in structural studies of the N_2-O_2 system:

1. From Raman spectra of the N_2 or O_2 vibrons and librons we want to deduce indirectly the $T-x$ and $p-x$ diagram. Clear spectral fingerprints appear for phase transitions upon plotting band frequency, bandwidth, or band intensity as a function of temperature T, pressure p, and/or concentration x.

2. The true concentration of liquid mixtures can be deduced from Raman cross-sections of the vibron modes (N_2 and O_2) and can be compared with the concentrations derived from partial pressures in the gas state.

3. The solubility of O_2 in N_2 phases can be determined from intensity ratios of Raman vibrons. This work contains the results from Raman spectra. In a forthcoming publication[20] we will present data from FTIR studies; this second technique provided more reliable data due to higher sensitivity.

4. Since high-pressure techniques (diamond anvil cell, membrane DAC) have been available for several years and since crystal growth is now achievable in these cells, we extend our studies to high-pressure phases too. We limited ourselves mainly to the N_2-rich side of the N_2-O_2 phase diagram. We hope to present a convincing explanation of the so-called "new phase" in Baer and Nicols[18] N_2-O_2 phase diagram at high pressures and room temperature. Our spectral analysis also delivers values such as environmental and matrix shift, which could be used to test mixed intermolecular potentials $U(N_2-O_2)$.

In the following section we will describe experimental details. In the discussion we will describe the procedure for extracting information about phase transitions from phonon and vibron spectra. Reproducibility of our data will be demonstrated from cooling−heating cycles. Then we will discuss the relation between phonon bandwidth and solubility, quantitatively determine the solubility from vibron band intensities and, finally, discuss several experimental details for high-pressure measurements.

2. Experimental Section

Nitrogen (99.999%) and oxygen (99.998%) were premixed in a large vessel in the desired composition via partial pressures at room temperature for several hours. The sample cell for measurements at ambient pressure was mounted on the tip of a closed-cycle helium cryostat (APD cryogenics Ltd.). The cell was built with special parts of copper and brass to produce a small (2−5 K) temperature gradient over the vertical axis for crystal growth, and was sealed with sapphire windows (thickness of sample $\sim$ 0.5 mm). The cell (cooled to T $\sim$ 65 K, where both components are liquid) was filled from the top via a heatable capillary. After filling, the optical cell and a short narrow capillary were sealed off from the gas vessel with a valve

(in order to avoid sublimation and to maintain the concentration ratio). The cell was slowly cooled to slightly below the liquid−solid transition point, and the sample was annealed at that temperature for several hours. All temperature changes of the sample were carried out at less than 2 K/h. The sample cell for high-pressure applications was a standard diamond anvil cell (DAC)[21] also mounted on the cold tip, as described above. To produce the desired sample mixture in the DAC we used the gas loading technique—the two gases were premixed in a gas vessel and, after several days, the DAC was loaded at the pressure of 100 bar, the pressure inside the DAC was elevated to 35−70 kbar, and the pressurized DAC dismounted from the gas loading system. In both cases, ambient pressure cell and DAC, a calibrated Si diode (accuracy ~ 0.1 K) was attached as close as possible to the sample thereby giving a sample temperature with an uncertainty of <2 K. A conventional system was used for Raman scattering, i.e., Ar-ion laser at 488 or 514.5 nm with 200−300 mW power at the sample and a triple monochromator with a resolution better than 2 cm^{-1}. For frequency calibration, we used a white light Fabry−Perot-interferogram in conjunction with atomic spectral lines and achieved an accuracy of ~0.7 cm^{-1}.

At ambient pressure we investigated six samples with different O_2 concentrations in N_2. One of our aims was to determine the real concentration of our solidified mixtures by an independent technique. Partial pressure was used to determine the concentration ratio of both gases. To check the actual concentration ratio in the liquid phase, we determined the intensity ratio of vibron Raman spectra of both components. The Raman cross-section for gaseous N_2 is defined to be one. Since there is no agreement in the literature as to the value of the Raman cross-section for gaseous oxygen (1.0−1.3),[22] we measured the cross-section in the liquid ourselves. Due to the fact that we maintain the concentration ratio from the liquid phase to the solid phases in our samples, we have to determine the Raman cross-section only in the liquid phase. To manage this, we filled the cell with liquid N_2, optimized the geometry, and measured the vibron band intensity. Taking care to avoid touching the optical components, we evacuated the cell, filled in liquid oxygen, and measured again at the same temperature (Figure 2a). We used a large spectrometer slit (~2 cm^{-1}), therefore we had only to compare the height of the band maximum to quantify the cross-section $\sigma(O_{2,liquid}) = 1.05$ with the appointed value $\sigma(N_{2,liquid}) = 1$. Figure 2b shows the vibron Raman spectra of a mixture $(N_2)_{0.80}$:$(O_2)_{0.20}$ by partial pressure. From the peak height we found the actual concentration to be $(N_2)_{0.62}$:$(O_2)_{0.38}$. The corrections in concentrations from gas to liquid phase are 16% → 6% ± 1%, 36% → 21% ± 4%, 50% → 35% ± 5%, 80% → 62% ± 6%, 90% → 78% ± 4%, and 94% → 81% ± 4%. These concentration corrections are shown in Figure 2c. Indirectly, we confirmed the condensation and boiling curves in the literature $T-x$ diagram.[23] Concentrations we will use in the following are the real concentrations found in the liquid due to Raman cross-sections at ambient pressure.

At high pressures, only two concentrations on the N_2-rich side were investigated, 2% and 7% of O_2 in N_2. Since the sample volume enclosed in the DAC is a closed volume, there was no need to correct for concentrations in the high-pressure case. Special care was taken that the initial pressure was not too high in order to ensure starting in a region of the fluid phase at room temperature.

In general, the band shape of Raman bands could be described by Voigt profiles. Larger spectrometer slits were used only where the Raman intensities were small, in which case the Gaussian contribution to band shape dominated. The usual band shape analysis (homogeneous bandwidth with Lorentzian profile, inhomogeneous with Gaussian profile) was not applied in the following since the bandwidths of Raman signals are broadened in mixtures.

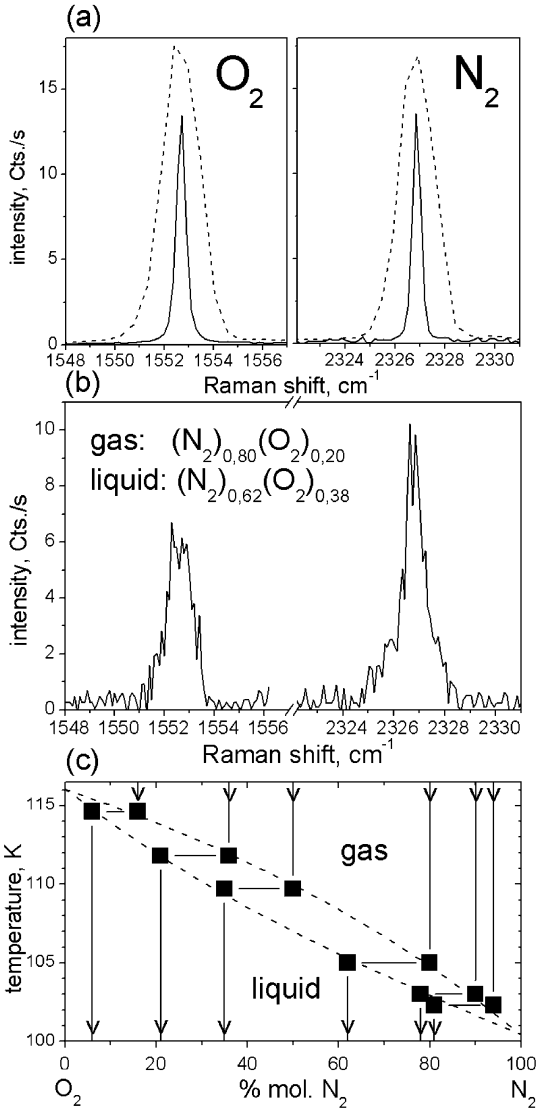

Figure 2. (a) Raman intensity of O_2 and N_2 stretching bands in the liquid state under the same conditions as calibration. Solid and dotted lines mean narrow and large spectrometer slits. (b) Raman intensities in the liquid mixture $(N_2)_{0.80}(O_2)_{0.20}$ from partial pressure in the gas state. The true concentration due to Raman cross-sections in the liquid is $(N_2)_{0.62}(O_2)_{0.38}$. (c) T−concentration diagram to demonstrate correction in concentrations: broken lines—boiling and condensation curves at 8 atm,[23] solid lines—our concentrations in gaseous and liquid phases. The transition points (closed squares) have been shifted to higher temperatures because of comparableness of our data (2.5 atm) with literature data at 8 atm.

Raman spectra in the vibron or phonon region were taken either during cooling cycles (T = 65 K → 14 K) or heating cycles or during both heating and cooling cycles to investigate reproducibility of Raman intensities (see also section 3.2.).

3. Results and Discussion

3.1. Phase Transitions. First we would like to demonstrate that it is possible to assign characteristic changes in phonon and vibron spectra to different phase transitions.

(a) Phonon Spectra. We selected two different nitrogen concentrations (x = 21% and 62%) to demonstrate phase

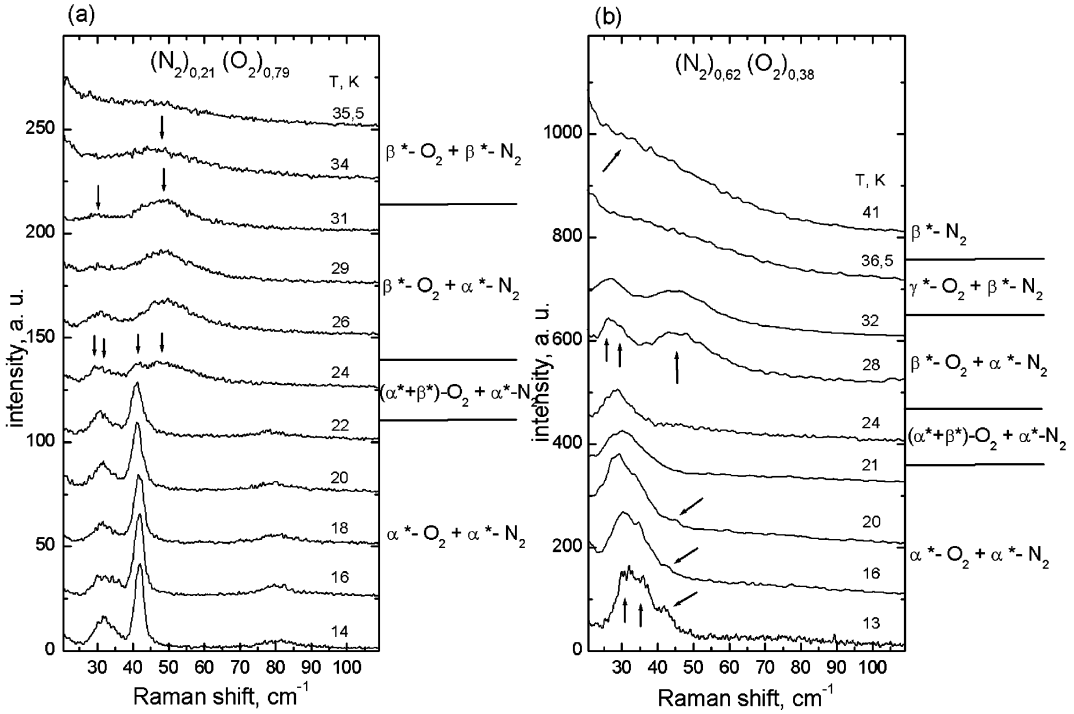

Figure 3. Raman spectra of the libron region as a function of temperature for two different concentrations: (a) $(N_2)_{0.21}(O_2)_{0.79}$, (b) $(N_2)_{0.62}(O_2)_{0.38}$. Arrows mark the position of libron modes. Phase boundaries obtained from our spectral analysis are indicated at the right side of diagrams ($\Delta T \sim \pm 1$ K, $\Delta\omega \sim \pm 1$ cm^{-1}).

transitions by changes in phonon spectra, in comparison with spectra of the pure systems. In pure α-N_2, libron modes were measured and assigned at 32 cm^{-1} (E_g), 37 cm^{-1} (T_g^-), and 60 cm^{-1} (T_g^+).[24] In α-O_2, librons are found in Raman spectra at 42 cm^{-1} (B_g) and 79 cm^{-1} (A_g).[25]

In Figure 3a, one can clearly identify the libron mode of α*-N_2 at 32 cm^{-1} between $T = 14$ and 22 K and both libron modes of α*-O_2 at 42 and 79 cm^{-1}. (The symbol * refers to the pure phase in a mixture.) At $T = 24$ K, the libron mode of β*-O_2 at about 50 cm^{-1} is also present; at $T \sim 26$ K, the librons of α*-O_2 could not be detected anymore. At $T = 34$ and 35.5 K, the librons of α*-N_2 disappear; those of β*-O_2 remain. The intensity of the low energetic part (<40 cm^{-1}) of the Raman spectrum increases, typical for the (plastic) β*-N_2 phase, similar to the characteristic Rayleigh wing of liquids.

Figure 3b presents the phonon spectra of the mixture $(N_2)_{0.62}$ $(O_2)_{0.38}$ in a similar way. The libron modes of α*- and β*-phases of N_2 and O_2 can be clearly distinguished in different regions. At $T > 36.5$ K, we assign the low-energy part of the Raman spectrum mainly to the broad Rayleigh wing of (plastic) β*-N_2.

Comparing both spectra (Figure 3a and b) for increasing temperature we can clearly confirm the phase pattern of the $T-x$ diagram (Figure 1) of both selected concentrations. On the other hand, some phase boundaries (e.g., β*-$O_2 \rightarrow \gamma$*-O_2) have to be shifted in temperature due to our results.

(b) Vibron Spectra. The vibron spectrum of $(N_2)_{0.78}$ $(O_2)_{0.22}$ in Figure 4 contains two bands at lower temperatures ($T < 39$ K) and only one band at higher temperatures ($T > 39$ K). The band at 1552.5 cm^{-1} is known from pure solid α-O_2 and β-O_2,[26] the band at 1555.5 cm^{-1} is known from matrix-isolated O_2 in α-N_2.[27] Therefore, the spectra at $T < 32.5$ K we assign to α*-O_2 (or β*-O_2) and α*-N_2. At $T \sim 34$ K we register a clear jump of the high-energy band (1555.0 cm^{-1}) to lower frequencies (1553.5 cm^{-1}) which we explain as the phase transition α*- to β*-N_2. Above $T \geq 40$ K we have recorded only one

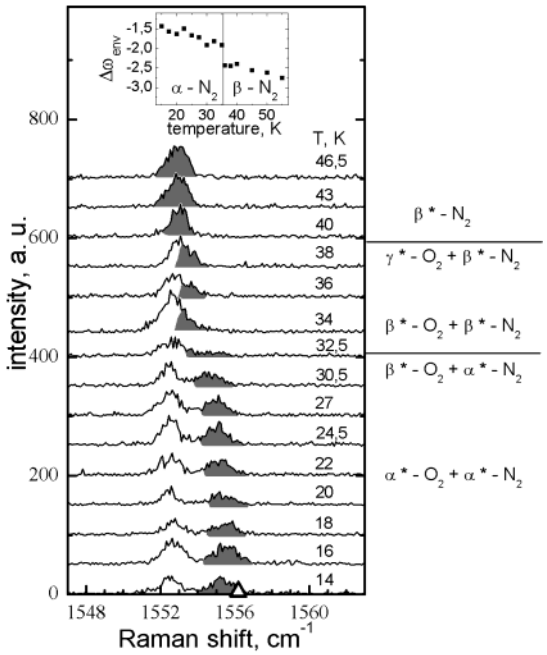

Figure 4. Raman spectrum of O_2 vibron as a function of temperature at a given concentration, $(N_2)_{0.78}(O_2)_{0.22}$. Shaded areas indicate the peak of the O_2-stretch in N_2. The temperature dependence of frequency corresponds to the oxygen gas value (Δ on frequency scale) plus nitrogen environmental shift (insert, from ref 31). Phase regions from our spectra are characterized at the right side of the diagram ($\Delta T \sim \pm 1$ K, $\Delta\omega \sim \pm 1$ cm^{-1}).

band in the oxygen vibron region. According to the $T-x$ diagram (Figure 1), there only exists β*-N_2 with a considerable O_2 component. Since we know the environmental shift $\Delta\omega_{env}$ of pure N_2 (see insert in Figure 4), we can qualitatively determine the expected frequency position of O_2 in N_2: oxygen gas value (1556.2 cm^{-1})[28] plus nitrogen environmental shift ($\omega_{solid} = \omega_{gas} + \Delta\omega_{env}$).[29] In general, the qualitative behavior of such an

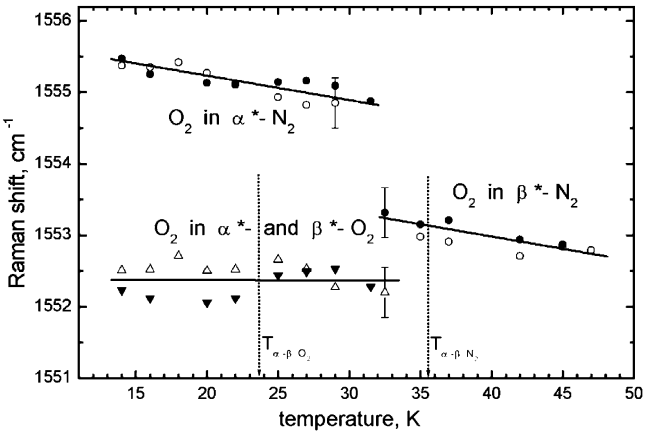

Figure 5. Frequency shift of the Raman active vibron of O_2 in the mixture $(N_2)_{0.81}(O_2)_{0.19}$ plotted as a function of temperature during cooling (closed symbols) and heating (open symbols). Vertical arrows indicate temperature of known phase transitions in pure systems: $T_{\alpha\beta}(O_2)$ at 23.8 K and $T_{\alpha\beta}(N_2)$ at 35.4 K.

environmental shift arises mainly from the crystal structure and the symmetry of occupied sites (in our case, N_2 in N_2 and O_2 in N_2: space group $Pa3$ with S_6 site symmetry—the same situation for both molecules). The value of the environmental shift itself comes mainly from the interaction potential between single molecule and matrix particles (in one case, N_2 in solid N_2; in the other case, O_2 in solid N_2). We could establish very good agreement between the results determined with this model and measured frequencies. In summary, changes in phonon or vibron spectra in comparison with the pure systems can be used to clearly determine phase transitions in the $T-x$ diagram.

3.2. Cooling−Heating Cycles and Reproducibility. To make reliable statements about phase diagrams ($T-x$, $p-T-x$), phase transitions, and solubility, one has to study samples in the thermodynamic equilibrium. In general, to check the quality of a sample by means of optical spectra, one uses the narrowness of the homogeneous bandwidth; however, all the bands are broadened in mixtures. Therefore, we carefully measured band frequencies and band intensities during cooling/heating cycles in order to check reproducibility and possible hysteresis effects, etc.

Technically speaking, we collected Raman spectra over a period of hours, so one temperature point (for one concentration) lasted about 1−2 days. For a whole cycle (14 K → 50 K → 14 K), more than one week was necessary. In general, we followed the following steps: after solidifying the mixture we cooled the sample very slowly (in order to avoid freezing-in of high-temperature phases), then we took spectra during heating, the sample was then maintained for 1 day at 50 K, and finally we collected spectra during cooling.

Figure 5 shows the temperature dependence of the oxygen vibron frequency for the mixture $(N_2)_{0.81}(O_2)_{0.19}$. Results for all other mixtures are equivalent. Both sets of data (cooling, heating) are on the same line $\omega(T)$ with minor scattering. The band at 1552.5 cm^{-1} is temperature-independent between 18 and 33 K, and we observe no frequency jump at the α*- to β*-O_2 phase transition ($T \sim 24$ K), as is expected. This band disappears in the spectra around 33 K. The band at 1555.5 cm^{-1}—assigned to O_2 in α*-N_2, later in β*-N_2—reveals a clear frequency jump of $\Delta\omega = 2.5$ cm^{-1} at $T_{\alpha}{}^{*}{}_{\beta}{}^{*}(N_2) = 32$ K ± 2 K, similar to the case of pure solid N_2 (at $T_{\alpha\beta} = 35.4$ K).[30] Since cooling and heating cycles deliver the same results, it follows that our samples are in thermodynamic equilibrium. We can clearly determine the temperature of phase transitions with an accuracy of $\Delta T < 1$ K from the vibron frequency jump.

We also measured the nitrogen vibron as a function of concentration and temperature during cooling/heating cycles. This procedure delivers spectra similar to those of the oxygen vibron. Remarkable here is that we could not detect spectra of N_2-vibrations in α*- or β*-O_2. Since the N_2 gas value is known to be 2330.7 cm^{-1} and the environmental shift of α-oxygen is ~ -9 cm^{-1},[31] we would expect a band at ∼2322 cm^{-1}. The fact that we did not observe a Raman band at this frequency proves indirectly that N_2 is not soluble in oxygen (see Figure 1) or only in concentrations below the detection limit (<1% in this case). In pure α-N_2 this vibron is split into two very narrow (<0.05 cm^{-1}) components: A_g at 2327.6 cm^{-1} and T_g at 2328.6 cm^{-1} with an intensity ratio $A_g/T_g \sim 4{:}1$.[30] In all our spectra of the N_2 vibron in O_2 (six concentrations), we observed around this frequency only one relatively broad band (bandwidth ∼ 2 cm^{-1}, accuracy in frequency ∼ 0.2 cm^{-1}) which has undergone a clear frequency jump of ∼ 1 cm^{-1} at $T_{\alpha}{}^{*}{}_{\beta}{}^{*}(N_2)$. This band was not affected in intensity, frequency position, or bandwidth by increasing oxygen concentration. Consequently, we can assign the band at ∼2328 cm^{-1} to a N_2 vibron in α*- or β*-N_2.

We can thus affirm from the reversibility of results that our samples were in thermodynamic equilibrium and can trust the results of our investigations.

3.3. Phonon Bandwidth and Solubility at Low Temperatures. One of the main discrepancies in two previously reported variants of the N_2-O_2 phase diagram at ambient pressure[14,15] is the discrepancy of the solubility at low temperatures (Figure 1). Both groups claim that <1% N_2 can be dissolved in α*-oxygen whereas Barrett et al.[14] claim a strong temperature-dependent solubility for oxygen in α*-N_2, going to zero at $T \sim$ 20 K; however, Baryl'nik et al.[15] assume the solubility to be almost constant up to about 18% O_2 in α*-N_2. Against the background of these controversial findings in the literature, our Raman spectra of librons will give a qualitative answer to the question of solubility.

In Figure 6a we present lattice mode spectra of α*-N_2 + α*-O_2 at several concentrations, including the spectra of both pure systems. In a way, we observe a systematic superposition of both phonon spectra with concentrations (Figure 6b). The oxygen librons remain narrow upon increasing the nitrogen concentration, and the bandwidths are comparable with those of pure O_2. On the other hand, the libron bands of N_2 broaden enormously in the mixture with oxygen.

From relative intensities of libron Raman spectra at one concentration (e.g., $(N_2)_{0.21}(O_2)_{0.79}$) (Figure 6a upper part) we cannot deduce the actual concentration (as was done for the vibron spectra of gaseous and liquid mixtures, Figure 2) because the Raman cross-section σ_{libron} for nitrogen and oxygen librons are unknown. A ratio of about 1.7(±0.3) to 1 was determined from spectra (sum of Raman intensities of E_g and T_g^- modes of N_2 compared to $I(B_g) + I(A_g)$ of O_2), and we see that $\sigma_{\text{libron}}(N_2) > \sigma_{\text{libron}}(O_2)$. The following arguments give a qualitative estimation of the ratio of libron Raman cross-sections. If one molecule vibrates along the normal coordinate q, then changes in polarizability ($\Delta\alpha/\Delta q$) determine the Raman cross-section. From the Clausius-Mosotti equation we can deduce a relation between polarizability and volume:

$$\alpha = 3\,\frac{\epsilon - 1}{\epsilon + 2}\,\frac{M}{\rho}\,\frac{\epsilon_0}{N_A} \sim V \qquad (1)$$

where ϵ represents permittivity, M molar mass, ρ density, ϵ_0 permittivity of vacuum, and N_A Avogadro's constant. $M/(\rho N_A)$ is thereby the volume V that an individual molecule occupies.

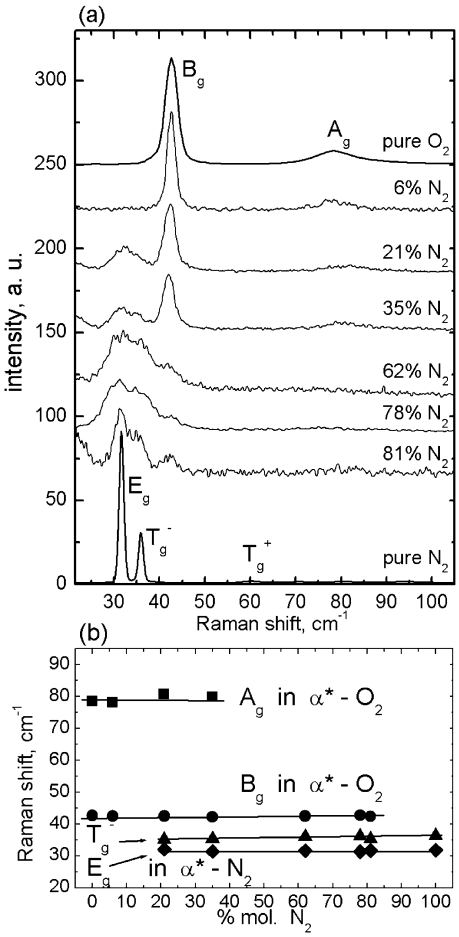

Figure 6. (a) Raman spectra of the libron region for different concentrations at $T = 14$ K. (b) Frequency shift of libron modes as a function of concentration at $T = 14$ K. Mode assignment in mixtures is based on the pure systems. (The two samples at 62% and 78% N_2 were produced by more rapid cooling than usual. Therefore, we see an additional broadening of libron bands.)

From the right side in eq 1, we derive the change in volume (or in polarizability) due to a free oscillation (Δq). The other factors are constant. Therefore, we can conclude that the Raman cross-section behaves more or less like the volume change:

$$\sigma \sim \frac{\Delta\alpha}{\Delta q} \sim \frac{\Delta V}{\Delta q} \tag{2}$$

In the case of the internal vibrations in the liquid phase (see section 2 and Figure 2), Raman cross-sections are nearly the same for both kinds of molecules: $\sigma_{\mathrm{vib,liquid}}(N_2)$ is defined to be 1, and we determine $\sigma_{\mathrm{vib,liquid}}(O_2) = 1.05$. For the vibrations of nitrogen and oxygen, we can estimate from intermolecular potential (6-12-Lennard-Jones) that Δq is about 0.016 and 0.017 Å, respectively. This implies volume changes (in our case a rotational ellipsoid of the charge distribution)[32] $\Delta V \approx 0.135$ Å^3 in the case of N_2 and $\Delta V \approx 0.140$ Å^3 for O_2. Consequently, it follows that $\sigma_{\mathrm{vib,liquid}}(O_2) \approx 1.03$, which is in good agreement with the experimental result (1.05).

Now we use the same arguments for the librations. It is known[33] that librating molecules in α-N_2 (24 K) performs changes in the angle of the molecular axis ($\langle\Theta^2\rangle^{1/2}$) of $\pm 16°$ and in α-O_2 (22 K) only of $\pm 9.6°$. The volume changes connected with these librations as above are $\Delta V \approx 5.658$ Å^3 for N_2 and $\Delta V \approx 2.955$ Å^3 for O_2. From these volume changes we get σ_{libron} (α-O_2) ≈ 1.9 with respect to $\sigma_{\mathrm{libron}}(\alpha\text{-}N_2) = 1$. The Raman cross-sections of librons are also in relatively good agreement with the experimental data from spectra ($\sim$1.7:1).

Changes in the bandwidth of librons (Voigt profile) on the N_2- or O_2-rich side are drastically different. Premixing O_2 in α^*-N_2, which is soluble, broadens the libron modes enormously because impurities perturb the electric quadrupole−quadrupole interaction of nitrogen and produce a strongly disturbed system. Premixing of N_2 in α^*-O_2 does not affect the O_2 libron because N_2 is not soluble (<1%) and therefore nitrogen is not present in the O_2-system.

In Figure 6b we plot the libron frequencies as a function of concentration. As stated, libron diagrams $\omega(x)$ are the simply superimposed libron diagrams of the individual systems. (The less intense A_g libron in α^*-O_2 is not observable at concentrations above 60% nitrogen but the intense B_g mode of α^*-O_2 exists at all concentrations. At small N_2 concentrations, the nitrogen libron modes are very weak and not detectable in spectra.)

From changes in the libron bandwidth we can derive some information about changing interactions, inhomogeneous broadening, and effects of disorder. We confirm that O_2 is soluble in α^*-N_2 and therefore, in this sense, favor the $T-x$ diagram of Baryl'nik et al.[15] (compare Figure 1). From libron spectra alone, it is only possible to make qualitative statements. In the next section we will use vibron spectra to give a quantitative analysis of solubility.

3.4. Vibron Intensity and Solubility of Oxygen in Nitrogen Phases. As we mentioned above there are considerable discrepancies in the literature concerning the solubility of oxygen in nitrogen phases, e.g., below 20 K it is quite inconsistent (see Figure 1): Barrett et al.[14] cite a negligibly small solubility and Baryl′nik et al.[15] claim that $\sim$18% oxygen can be solved in α^*-N_2. Our analysis of Raman spectra in the vicinity of the oxygen vibron allows us to make a more quantitative statement than in the case of libron spectral analysis, and it provides a possible explanation of the aforementioned discrepancy on the basis of data from structural analysis.

Since the integrated Raman intensity is

$$I \sim \omega^4 \cdot \Delta\alpha^2 \cdot c(\%) \tag{3}$$

and since we know the values of ω and $\Delta\alpha$, we can estimate real concentrations by evaluation of the relative intensities.

Figure 7 shows the oxygen vibron as a function of concentration at two different temperatures: at $T = 14$ K (Figure 7a) and at $T = 42$ K (Figure 7b). The true bandwidth of vibrons in pure oxygen is very narrow (<0.1 cm^{-1},[26] high-resolution Raman spectra of pure α-O_2 and γ-O_2 are plotted with broken lines in Figure 7), whereas the resolution in our spectra of the mixed systems was $\sim$2 cm^{-1}. Therefore, the spectral features at higher temperatures (Figure 7b) must contain at least two contributions due to different surroundings (N_2/O_2) or due to the doublet in pure γ-O_2 (1552 and 1553 cm^{-1}, intensity ratio 3:1). In the first step we discuss the low-temperature spectra (Figure 7a).

The Raman spectrum of $(N_2)_{0.81}(O_2)_{0.19}$ at $T = 14$ K contains two clearly separated bands. We assigned (see section 3.1.b) the band at 1552.25 cm^{-1} to the O_2 vibron in α^*-O_2 and the one at 1555.5 cm^{-1} to the O_2 vibron in α^*-N_2. The integrated Raman intensities are 16.5 au and 5.2 au. Now we would like to answer the question as to how many oxygen molecules in the mixture $(N_2)_{0.81}(O_2)_{0.19}$ are dissolved in α^*-N_2.

From the Raman band intensity ratio $R = [I(O_2 \text{ in } N_2)]/[I(O_2 \text{ in } O_2) + I(O_2 \text{ in } N_2)] = 5.2 \text{ au}/(16.5 \text{ au} + 5.2 \text{ au}) \approx 0.24$, we find the fraction of O_2 molecules in α^*-N_2 in comparison to all

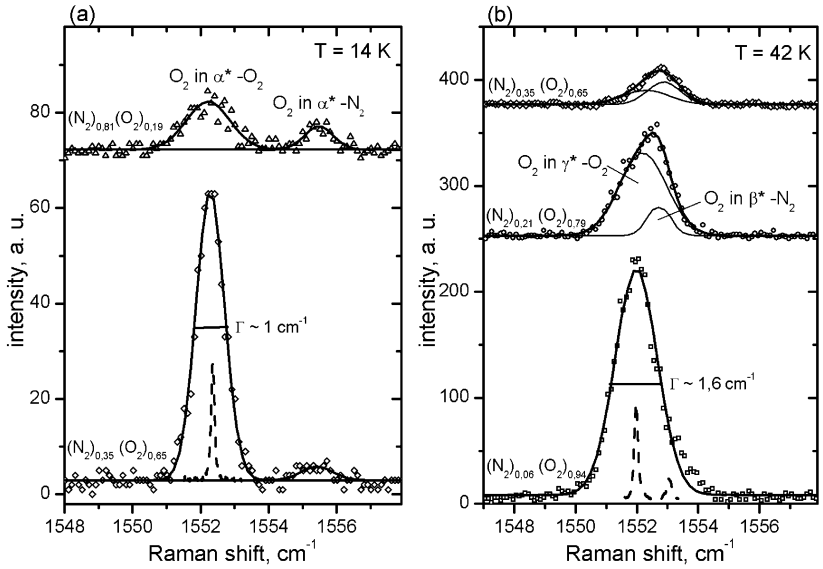

Figure 7. Raman spectra of O_2 internal vibrations: (a) for two different concentrations at the lowest temperature; (b) for three different concentrations at 42 K. High-resolution Raman spectra of pure α-O_2 and γ-O_2 are added for comparison (broken line at bottom).[26]

O_2-molecules in the mixture (or 4.56% = 0.24 × 19% of all the molecules in the mixture). This sample contains regions of α*-O_2, in which practically no (<1%) N_2 is dissolved, and regions of α*-N_2 that contain a certain amount of oxygen molecules. Thus, almost all (>99%) N_2 molecules in this mixture are α*-N_2. We can therefore define the solubility of oxygen in α*-N_2 as $S = R{\cdot}c(O_2)/[R{\cdot}c(O_2) + c(N_2)]$. Consequently, in our case, $S = 0.24{\cdot}19\%/(0.24{\cdot}19\% + 81\%) = 5.3\%$ which means that only 5.3% of O_2 is dissolved in α*-N_2 in the sample $(N_2)_{0.81}(O_2)_{0.19}$.

The Raman spectrum of $(N_2)_{0.35}(O_2)_{0.65}$ at $T = 14$ K (Figure 6a, lower part) can be analyzed by the same procedure. The stronger Raman band (63.5 au) is assigned to the O_2 vibron in α*-O_2 and the weaker one (3.4 au) to O_2 in α*-N_2. The intensity ratio is $R = I(O_2 \text{ in } N_2)/[I(O_2 \text{ in } O_2) + I(O_2 \text{ in } N_2)] = 3.4$ au/(63.5 au + 3.4 au) ≈ 0.05. Therefore the solubility in this case is $S = 0.05{\cdot}65\%/(0.05{\cdot}65\% + 35\%) = 8.5\%$, that means 8.5% of O_2 is dissolved in α*-N_2 in the mixture $(N_2)_{0.35}(O_2)_{0.65}$.

From Raman spectra in different mixtures we found that the solubility of O_2 in the α*-N_2 at low temperatures is in the range of 5.3%−8.5%. We believe more in the lower value because this value is closer to that obtained by FTIR studies,[20] because the weak Raman band (lower part of Figure 6a) produces some additional uncertainty and—last but not least—the sample $(N_2)_{0.35}(O_2)_{0.65}$ was grown more rapidly (at a larger cooling rate) than the sample $(N_2)_{0.81}(O_2)_{0.19}$.

Finally, we compare the solubility won from our Raman spectra (5 −8%) to those inferred from structural investigations (Barrett et al.[14] claim about 0% solubility at this temperature and Baryl'nik et al.[15] about 18%). There is strong evidence that the discrepancy in the literature is due to differences in sample preparation. For structural analysis, a very disperse polycrystalline sample is preferable, so Baryl'nik et al.[15] produced their samples by condensing on a cold substrate, then the samples were annealed at relatively low temperatures (∼30 K) for only $1^1/_2$ h. On the other hand, Barrett et al.[14] grew their samples from the liquid phase. To avoid segregation, the authors cooled their samples down to temperature in just 5 min, and we are convinced that homogenization or annealing did not occur, because diffusion processes at lower temperatures are very slow. Thus we doubt that any of the two kinds of the N_2-O_2 phase diagram describe the situation at equilibrium conditions. One of the most important aims of our spectroscopic studies (Raman + infrared) was to obtain an equilibrium phase diagram of the N_2-O_2 mixture, so we produced and cooled our samples carefully and controlled their quality over days. Therefore, we believe in the quality of our findings.

We now discuss the spectra at higher temperature (Figure 7b). At $T = 42$ K both kinds of phase diagram (see Figure 1) claim a rather high solubility of oxygen in the β*-N_2 phase (Barrett et al. 25−30%, Baryl'nik et al. ∼50%). We apply our method of deducing solubility from Raman spectra in this case too. But our aim is more to check our method than to obtain a precise value of solubility. Figure 7b shows Raman spectra of the O_2 vibron in different mixtures $(N_2)_x(O_2)_{1-x}$ at temperatures around 42 K. With known vibron frequencies we can model the broad asymmetric Raman band around 1552−1553 cm^{-1} with two bands: the band at 1552.2 cm^{-1} can be assigned to O_2 in γ*-O_2 (in fact a doublet but not resolved here, see the spectrum of pure γ-O_2 at bottom of Figure 7b) and the band at 1552.7 cm^{-1} to O_2 in β*-N_2 (see Figure 4). At these temperatures, and for all concentrations, we can exclude the presence of β*-O_2 because we do not register any of the libron modes below 100 cm^{-1} which are characteristic for the ordered phases. At small N_2 concentrations [$(N_2)_{0.06}(O_2)_{0.94}$, lower part of Figure 7b] one can see only one broad, slightly asymmetric (high-frequency) Raman band. Therefore, we deduce that all oxygen is present in γ*-O_2 (6% of N_2 is well below the solubility of N_2 in γ*-O_2 which is believed to be 10−12%). The band of the next mixture—$(N_2)_{0.21}(O_2)_{0.79}$—is broad and asymmetric on the low-frequency side. The Raman band intensity of the O_2 vibron is 75 au in γ*-O_2 and 14 au in β*-N_2. Following the same procedure as before (with the assumption that solubility of N_2 in γ*-O_2 is ∼10%, see Figure 1) we find that 40−45% of O_2 is dissolved in β*-N_2, a value which is between the results of Baryl'nik et al.[15] and Barrett et al.[14] From the spectrum of the $(N_2)_{0.35}(O_2)_{0.65}$ mixture we obtain a solubility of 45−50%. Increasing the amount of N_2 in the mixtures, the Raman band on the lower frequency side of the spectrum (assigned to O_2 in γ*-O_2) disappears.

We estimate errors in integrated Raman band intensities of about 5−10%, in solubility of N_2 in oxygen phases of less than ±2%, and an uncertainty in concentration obtained from Raman cross-sections of between 1 and 6% for different mixtures.

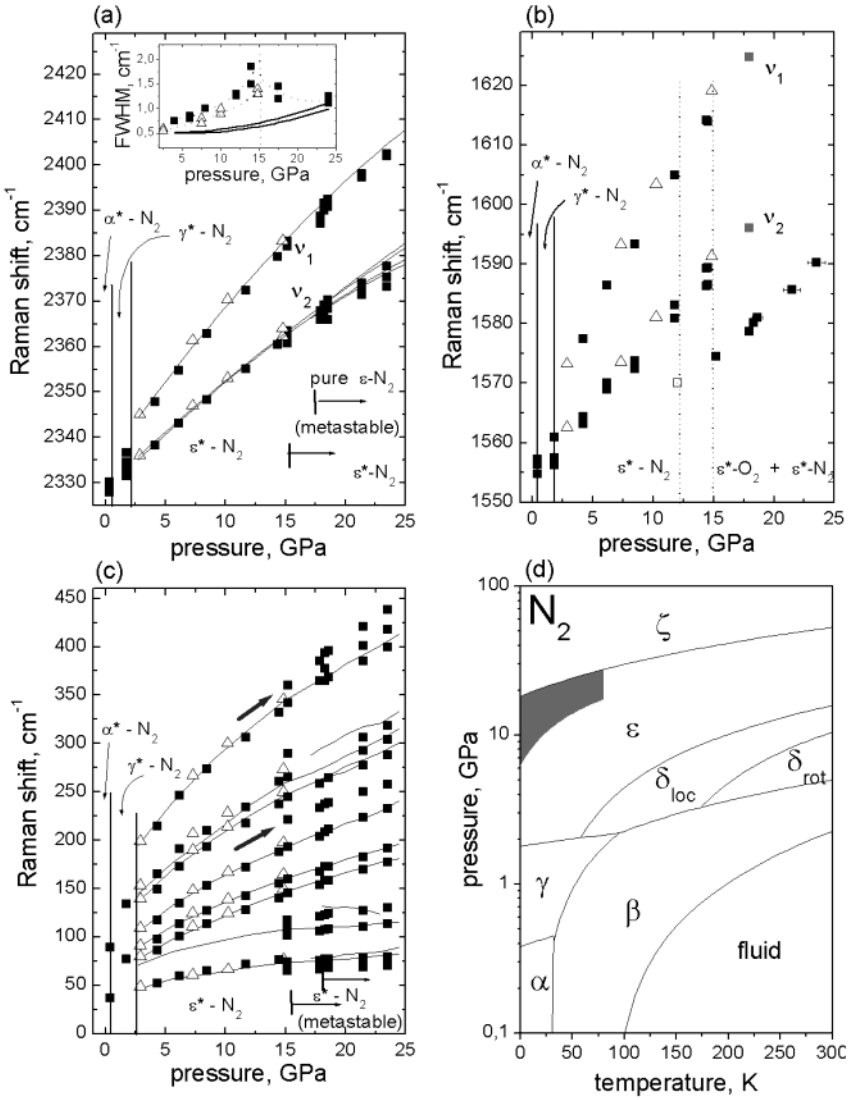

Figure 8. Frequency shifts of N_2-vibrons (a), O_2-vibrons (b), and librons (c) as a function of pressure at $T = 19$ K for different O_2 concentrations (open triangles: 2% and closed squares: 7% O_2). In (b) data points assigned to the ν_1 band describe the position of an asymmetric band, whereas ν_2 data points represent a doublet. Solid lines in all diagrams describe the pressure dependence in pure N_2.[34] Vertical lines separate different high-pressure phases of N_2 known from the $p-T$ diagram of N_2 (d).[34] Mode assignments of vibrons and librons are in accordance with the pure systems. Insert in Figure 8a shows the bandwidth of the nitrogen vibrons ν_1 and ν_2 as a function of pressure for pure and O_2-doped solid nitrogen.

Therefore, the total error in solubility is less than ±3% for low temperatures and ±7% for higher temperatures. In general, concentration-dependent Raman studies deliver rather poor spectra. Nevertheless, we are convinced that we are able to determine the real concentration ratios and solubility from spectroscopic information while the samples are preserved at thermodynamic equilibrium. A more detailed study of the ambient pressure phase diagram of N_2-O_2 by infrared spectroscopy will be presented later.[20]

3.5. High-Pressure Aspects. We present here high-pressure data ($p < 25$ GPa) of the nitrogen−oxygen system at low and room temperature. Since, especially for pure N_2 at high-pressure, the libron spectra are quite rich, and since the bandwidth of libron modes increases enormously even by doping with 10% O_2 (besides pressure broadening) we focus here only on the N_2-rich side (2% and 7% of O_2 in N_2). We will give an explanation for the so-called "new phase" in the $p-T-x$ diagram proposed by Baer and Nicol.[18] At the end of this section we also describe Raman spectra on the O_2-rich side as a control experiment.

In Figure 8 we present the frequency shifts of the N_2 vibron on pressure variation (<25 GPa, Figure 8a), of the O_2 vibron (Figure 8b), and of the librons (Figure 8c), respectively, of both mixed systems with 2% and 7% O_2 in N_2. All spectra—vibrons as well as phonons—are quite similar to those of the pure nitrogen system at high pressure. For comparison, we plotted $\omega(p)$ for pure N_2 as solid lines; vertical lines indicate phase transitions in the known $p-T$ diagram of N_2,[34] see Figure 8d. The assignment is from the literature:[35] the ϵ-phase of N_2 is described by a multisite rhombohedral structure ($R\bar{3}c$) having eight molecules per structural unit cell. Six molecules are located on site 6e with C_2 symmetry, having two Raman active modes of A_{1g} and E_g symmetry which are detected as one Raman band (ν_2:($\nu_{2a} + \nu_{2b}$)) with a shoulder at the high-frequency side. Two molecules are on site 2b with S_6 symmetry with one Raman active mode A_{1g} observed in Raman scattering at higher frequencies (ν_1). At the same pressure, but at higher temperatures—in the δ-phase—the structure ($Pm3n$) is similar to that of the ϵ-phase but more symmetric. The vibron band ν_2 in the δ-phase belongs to six disklike disordered N_2 molecules on site 6c with

D_{2d} symmetry in the cubic cell, whereas the band ν_1 belongs to two sphere-like disordered N_2 molecules on site 2a with T_h symmetry. In the high-temperature δ-phase, no librons are observable because of the orientational disorder of molecules. In the ϵ-phase of N_2, where the molecules are orientationally ordered and the former cubic cell is slightly rhombohedraly distorted, eight libron modes ($7\ E_g + 1\ A_{1g}$) could be detected.

In the pressure range below 15 GPa, the spectra of the N_2 vibron in the oxygen-doped N_2 matrix (see Figure 8a) shows a similar splitting in frequency as in the pure ϵ-N_2; the intensity ratio $I(\nu_2)/I(\nu_1) \approx 3{:}1$ is not affected by 2% or 7% O_2 in N_2. Therefore, the assignment remains as in the case of pure N_2: ν_2 originates from molecules located at sites of symmetry C_2 in solid ϵ*-N_2 and ν_1 from those at sites of symmetry S_6. We could also clearly identify the two expected librons in γ*-N_2 and the 8 expected librons in ϵ*-N_2 in our spectra of O_2-doped N_2 matrixes (Figure 8c). Any further lattice excitations, which do not belong to ϵ*-N_2, could not be observed in the pressure range below 15 GPa. The spectra of the O_2-vibration in the oxygen-doped N_2 matrix (see Figure 8b) deliver very similar splitting into ν_1 and ν_2 as for the N_2 vibron. In addition, the pressure dependencies $\nu_1(p)$ and $\nu_2(p)$ are similar and the splitting $\Delta\nu(p) = \nu_1 - \nu_2$ is of the same order of magnitude as that of the N_2 vibron. Therefore, we assign the ν_2 Raman band to O_2 molecules in ϵ*-N_2 at 2a sites of C_2 symmetry and the ν_1 band to those in ϵ*-N_2 at 6c sites of symmetry S_6. The intensity ratio of these bands $I(\nu_2)/I(\nu_1)$ (3:1 due to occupation of different sites at low pressure) tends to the value 1:1 at higher pressure. Since the O_2 molecules are more or less isolated in the ϵ*-N_2 matrix (doped by 2% or 7% of O_2) and since the intensity ratio is the same for both mixtures, the so-called vibron−vibron resonant transfer coupling, as in the case of pure O_2 with $Pm3n$ structure (γ-phase),[36] can be neglected. Thus we can interpret this change in intensity ratio by the fact that fewer O_2 molecules are embedded on 2a sites. Vibrons from O_2 molecules in their own phase could not be detected.

We could clearly identify a systematic effect of O_2 concentration on spectra. The frequencies of the N_2 vibron or the O_2 vibration bands decrease on doping from 2% to 7% of O_2. The insert in Figure 8a shows the bandwidth as a function of pressure for the ν_1 and ν_2 bands of N_2 in pure ϵ-N_2 as solid lines.[34] Data points for 2% O_2 (open triangles) and 7% O_2 (closed squares) in ϵ*-N_2 clearly demonstrate an additional increase in bandwidth—besides pressure broadening—due to impurities (O_2 molecules), which we explain as inhomogeneous broadening resulting from disorder.

Summarizing the above results, we can state that 2% and even 7% O_2 are soluble in ϵ*-N_2 in the pressure range below 15 GPa.

At pressures above 15 GPa both Raman bands of nitrogen—ν_2 modes (ν_{2a}, ν_{2b}) as well as the ν_1 mode—change to asymmetric bands or even to doublets. For comparison, in the pure N_2 system the ν_{2a} and ν_{2b} bands split into 4 bands before the phase transition $\epsilon-\zeta$ occurs at ~25 GPa. From experiments in pure nitrogen we know that, in the range 17−25 GPa at low temperatures, the ϵ-phase exists only in the metastable form (shaded area in Figure 8d).[34] From bandwidth studies,[37] we know that one can reach the stable form of pure ϵ-N_2 structure only if pressure is applied at temperatures above room temperature. Therefore, we can explain the additional splitting of N_2 vibron lines in our mixtures by metastability of ϵ*-N_2 (e.g., slight changes in structure, doubling of cell, etc.). The metastable range in our mixtures (ϵ*-N_2) starts at ~15 GPa in comparison with pure ϵ-N_2 at ~17 GPa (Figure 8a and 8c). This enlargement of the metastable range must be caused by impurities (O_2 molecules). In this pressure range, we also observe an additional splitting of the N_2 libron modes (see Figure 8c) in mixtures—a splitting which is similar to the splitting of libron modes in metastable pure N_2. However, we recognize two additional narrow lines (at ~220 cm^{-1} and ~350 cm^{-1}, marked by arrows in Figure 8c) in libron spectra at pressures higher than 15 GPa which cannot be explained by features of (metastable ϵ*-) nitrogen.

For the O_2 vibron we observe a drastic change at pressures above 15 GPa and 7% O_2 (Figure 8b). The ν_2 and ν_1 bands disappear and a new band appears at lower frequencies. This spectral feature of the vibron modes was the reason Baer and Nicol[18] called this $p-T-x$ region a "new phase". The frequency of the O_2 vibron also increases with pressure: $\nu(p = 15\ \text{GPa})$ ~1575 cm^{-1} to $\nu(p = 24\ \text{GPa})$ ~1590 cm^{-1}. Since we know from N_2 vibron and librons that there is no serious change in nitrogen structure in our mixtures at 15 GPa, this additional line in the energy range of the O_2 vibration must be a feature of oxygen alone. Further support for this assumption is the disappearance of the additional broadening of N_2 vibron lines between 15 and 25 GPa (see insert in Figure 8a), which we associated with impurities (oxygen molecules). This means that the phases separate above 15 GPa. This big change (demixing) in the solid at ~15 GPa depends strongly on temperature and time. The ν_2 and ν_1 lines disappear at several GPa higher than the phase transition by fast pressurizing at room temperature (gray squares in Figure 8b). They also disappear during soaks at pressures near the phase transition. At low temperatures, these effects are stronger than at room temperature, as expected. This critical pressure varies between 12 and 15 GPa, depending on raising or lowering (open squares) the pressure in the DAC. The demixing may happen simply because this phase is more stable. However, it is also possible that certain processes in (metastable) nitrogen could cause such an effect.

Next we would like to compare these additional features in spectra above 15 GPa, i.e., librons at 220 cm^{-1} and at 350 cm^{-1} and the vibron at 1575 cm^{-1}, with spectra of pure O_2 to find an explanation for this "new phase". The phase transition δ- to ϵ-O_2 at 8 GPa ($T \sim 20$ K) is known; the Raman band of the O_2 vibron in pure O_2 increases linearly with pressure in the δ-phase, at the phase transition δ- to ϵ-O_2 the vibron frequency decreases from 1580 to 1575 cm^{-1},[36] followed by a linear increase with pressure ($\Delta\nu/\Delta p \sim 2.17$ cm^{-1}/GPa) in the ϵ-phase.[38] Libron Raman bands are at 180 cm^{-1} and at 380 cm^{-1} ($p = 20$ GPa, $T = 300$ K).[38] We believe that these additional features in our spectra of mixed systems at high pressure (one vibron, 2 librons) are due to ϵ*-O_2 formed by a demixing of O_2 from the ϵ*-N_2. Nevertheless, we must explain why the O_2 vibron in our mixture is situated around 10 cm^{-1} lower than in the pure ϵ-O_2 and why both librons in the mixture possess higher frequencies in comparison to pure ϵ-O_2. In our picture there is a certain amount of nitrogen molecules embedded in ϵ*-O_2—there are not enough N_2 molecules dissolved in ϵ*-O_2 to be detected by Raman spectroscopy but sufficient to disturb the interaction between oxygen molecules. Therefore, the resonance shift of the oxygen vibrons is partially diminished by N_2 impurities in the ϵ*-O_2. For pure ϵ-O_2 we expect a positive resonance shift of about 10 wavenumbers at these pressures.[31] Consequently, the vibron in ϵ*-O_2 (containing a small amount of N_2) should have a lower frequency than in pure ϵ-O_2.

The interaction between oxygen molecules is disturbed by nitrogen molecules which additionally hinder the collective libration (i.e., higher force constant). Accordingly, the "hin-

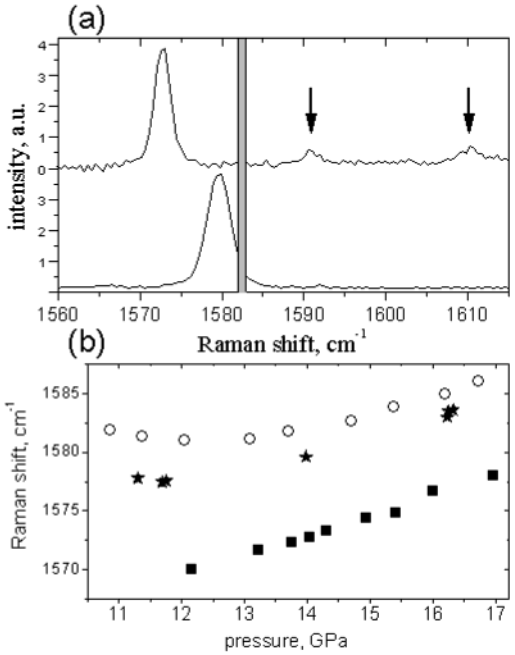

Figure 9. Room-temperature data of the oxygen vibron: (a) Spectra at $p = 14.0$ GPa in the mixture $(N_2)_{0.93}(O_2)_{0.07}$ (upper part) and in $(N_2)_{0.02}(O_2)_{0.98}$ (lower part). The peaks at ~1590 and ~1610 cm^{-1} in the nitrogen-rich mixture (marked by arrows) originate from oxygen molecules occupying two different sites in ϵ*-N_2. Other peaks in both mixtures lie at lower frequencies than the oxygen vibron in pure ϵ-O_2 at this pressure (gray bar). (b) Pressure-dependent frequency evolution of O_2 vibron in the ϵ*-phase of different O_2-N_2 solutions in pure oxygen (open circles, ref 39), in $(N_2)_{0.02}(O_2)_{0.98}$ (stars), and in the "new phase" (squares), which we assume to be nitrogen-doped (≥5%) ϵ*-O_2 in the mixture $(N_2)_{0.93}(O_2)_{0.07}$.

dered" librations in ϵ*-O_2 are at higher frequencies than those of unperturbed librations in pure ϵ-O_2.

A control experiment in the oxygen-rich mixture $(N_2)_{0.02}$-$(O_2)_{0.98}$ confirmed the above hypothesis. Figure 9 shows the O_2 vibron spectrum at $T = 300$ K in different mixtures (a), and the pressure dependence of this mode in different mixtures (b). The position of the oxygen vibron in pure ϵ-O_2 at $p = \sim 14$ GPa and $T = 300$ K is shown by a gray bar in Figure 9a and its pressure dependence by open circles in Figure 9b. The O_2 vibron in $(N_2)_{0.02}(O_2)_{0.98}$ lies at lower frequencies with respect to the pure case (lower part in Figure 9a); the O_2 vibron in ϵ*-O_2 demixed from the $(N_2)_{0.93}(O_2)_{0.07}$ system and containing some N_2 molecules as impurities is also on the low-frequency side (upper part in Figure 9a, closed squares in Figure 9b). Therefore we believe that the new phase observed by Baer and Nicol[18] is simply ϵ*-O_2 with ~5% of N_2 dissolved in it.

To conclude, we can clearly identify the phase transitions of N_2 doped by O_2 from $\alpha^* \rightarrow \gamma^* \rightarrow \epsilon^*$ nitrogen phases according to the $p-T$ diagram of pure N_2 (Figure 8d) as a consequence of frequency jumps or additional splitting and changes in bandwidth of vibron and libron modes. We pointed out that we are able to establish a limited $p-T-x$ diagram by optical spectroscopy. Furthermore, we could explain the real composition of that phase, which was previously called a new phase. To complete the $p-T-x$ phase diagram of N_2-O_2, additional concentration-dependent spectroscopic and/or structural studies are necessary.

3.6. Shift of Vibron Frequency in Binary Mixtures and Related Interaction Potential. To model spectroscopic results on binary mixtures by means of theoretical methods, one needs to know the intermolecular potentials of such systems. The discussion of intermolecular combined potentials was applied initially to the matrix-isolated case,[40] i.e., with less than a few percent type A molecules in a matrix of type B molecules. Since the matrix shift of vibrational frequency (gas-phase value minus measured value in the matrix) is typically in the order of thousandths of the respective excitation energy, the modeling by combined potentials was not too convincing. Application of pressure ($p < 20$ GPa) causes these frequency shifts to increase dramatically, typically ~50 cm^{-1}. In addition, application of pressure varies geometrical distances between host molecule A and matrix particles B, which enables one to test the combined potential as a function of the nearest-neighbor distance.

It is necessary, in this context, to discuss the pressure-dependent vibron frequency shifts of N_2 and O_2 in the two mixtures 2% and 7% O_2 in N_2 with respect to the pure N_2 system. The solid shift in pure systems has two contributions:[5b,31,41]

$$\Delta\omega_{solid} = \omega_{solid} - \omega_{gas} = \Delta\omega_{env} + \Delta\omega_{res} \qquad (4)$$

The first term on the right side mirrors the change in energy as a result of the interaction of a single molecule with its surrounding (environmental shift $\Delta\omega_{env}$), the second term arises due to an exchange of excitations between identical molecules (resonance shift $\Delta\omega_{res}$).[31] In the ideal matrix isolated case—one molecule of type A in a matrix of type B molecules—there is no resonance interaction between A molecules; therefore, the solid shift in such a system is

$$\Delta\omega_{solid} = \Delta\omega_{matrix} = \Delta\omega_{env} \qquad (5)$$

Doping the N_2 matrix by 2% (or 7%) O_2 means that the probability of one O_2 molecule having another O_2 molecule as a nearest neighbor is relatively low—less than 10% (or 20%).[42] Therefore, one can neglect the resonance interaction in these low-doped mixed systems, and thus we can apply the matrix-isolated case to good approximation.

To compare the environmental shift in the mixed system (N_2-O_2) to that in the pure system (N_2), we have to take into account at least three effects: (1) the embedded impurity molecules (O_2) will change the nearest neighbor distance in the nitrogen matrix—a static lattice relaxation, (2) the force constants of the isolated oxygen and nitrogen molecules are different [$\omega_0(N_2) \neq \omega_0(O_2)$], and (3) the pair interaction potentials $U(N_2-N_2)$, $U(O_2-O_2)$, and $U(N_2-O_2)$ are different. In the following we discuss the influence of these three effects.

In Figure 8a we plotted the frequency of the nitrogen vibron versus pressure in pure nitrogen and in N_2 doped by 2% and 7% O_2. The frequency shift of the N_2 vibron is less than 3 cm^{-1} (depending on the O_2 concentration). Taking into account that the pressure-induced shift is ~50 cm^{-1}, we contend that static relaxation—embedding 2% or even 7% O_2 in N_2—is effectively insignificant. Next, we have to consider the influence of the different force constants to obtain an assumption for the remaining influence of the combined potential. Therefore, we have to compare the matrix shift of the oxygen vibration in N_2 with that by the nitrogen vibron in the pure system.

Unfortunately, the environmental shift of pure $^{14}N_2$ as a function of pressure is not known. However, the experimental pressure dependence of the vibration frequency of the $^{14}N^{15}N$-isotopomers in $^{14}N_2$ matrix has been published[43] and was also investigated in the present work. By proper mass scaling of these data ,we could obtain the environmental shift of $^{14}N_2$ in the N_2 matrix (see Figure 10a). In the δ-phase of N_2, we observe two Raman vibrons: the band ν_2 assigned to the six disklike

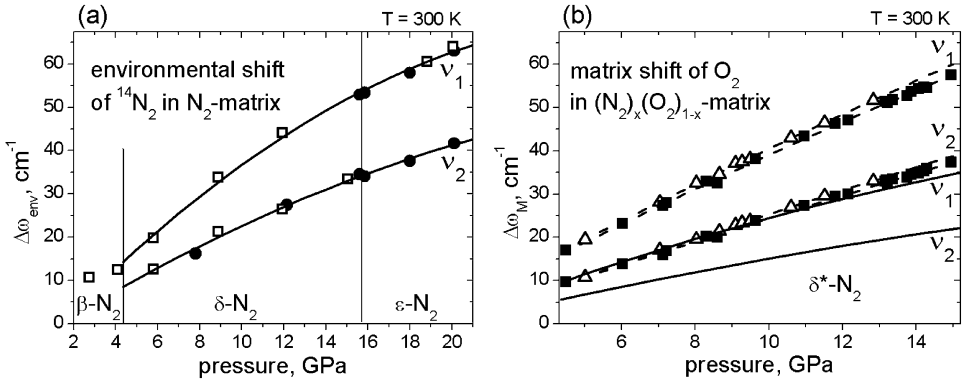

Figure 10. (a) Environmental shift of the ν_1 and ν_2 Raman bands of $^{14}N_2$ in a N_2 matrix as a function of pressure deduced from the Raman data of the $^{14}N^{15}N$-isotopomers in a N_2 matrix (closed circles, ref 43; open squares, our measurements). (b) Environmental shift of the O_2 vibration in $(N_2)_{0.98}(O_2)_{0.02}$ [open triangles] and $(N_2)_{0.93}(O_2)_{0.07}$ [closed squares] as a function of pressure (broken lines; fit parameters are shown in Table 1). Solid lines are environmental shift of the ν_1 and ν_2 Raman bands of $^{14}N_2$ in N_2 (from Figure 10a) multiplied by the ratio $\omega_{gas}(O_2)/\omega_{gas}(N_2)$.

TABLE 1: Parameters of Quadratic Fit Functions ($\Delta\omega = a{\cdot}p^2 + b{\cdot}p + c$) for the Pressure Dependence of Frequency Shift Data in Figure 10 (broken lines in Figure 10b and solid lines in Figure 10a)

mode	shift	mixture $(N_2)_x(O_2)_{1-x}$	a cm^{-1}/GPa^2	b cm^{-1}/GPa	c cm^{-1}
ν_1	$\Delta\omega_{matrix}$	$x = 0.93$	−0.035	4.58	−3.19
ν_2	$\Delta\omega_{matrix}$	$x = 0.93$	−0.009	2.85	−3.19
ν_1	$\Delta\omega_{matrix}$	$x = 0.98$	−0.027	4.60	−2.83
ν_2	$\Delta\omega_{matrix}$	$x = 0.98$	−0.020	3.19	−4.59
ν_1	$\Delta\omega_{env}$	$x = 1.00$	−0.087	5.21	−6.74
ν_2	$\Delta\omega_{env}$	$x = 1.00$	−0.041	3.08	−4.15

disordered N_2 molecules and the band ν_1 assigned to the two sphere-like disordered N_2 molecules per unit cell.

Now we are able to put all relevant spectroscopic data together (Figure 10b). If we scale the environmental shift data from Figure 10a by the square-root of the ratio of the force constants ($\Delta\omega_{env}(N_2){\cdot}(\omega_{gas}(O_2)/\omega_{gas}(N_2))$) we get the solid lines in Figure 10b. The broken lines in Figure 10b are the matrix shifts of the O_2 vibration as a function of pressure for the two cases $(N_2)_{0.98}(O_2)_{0.02}$ and $(N_2)_{0.93}(O_2)_{0.07}$. Since we have taken all other effects into consideration, the significant difference between solid and broken lines in Figure 10b is due only to the influence of the combined intermolecular potential. At any selected pressure, e.g., 10 GPa, the difference in shift between the doped case and the pure case for the ν_1 mode is about 12 cm^{-1}, and the difference for the ν_2 mode is about 8 cm^{-1}. The particulars shown in Table 1 allow us to map out a data record in the pressure range from 4 to 15 GPa.

Due to the fact that no real knowledge of intermolecular potentials in binary mixed systems exists up to now, and since the formulas combining the potential with environmental shift are relatively simple and well-known (e.g., eq 3a in ref 31), it should be interesting for theoretical approaches to test new combined intermolecular potentials (effective potential energy of the crystal) with our set of experimental data (Table 1).

4. Conclusion

Samples with different concentrations $(N_2)_x(O_2)_{1-x}$ were grown and we performed Raman studies at ambient pressure and low temperatures and at high pressures at both room and low temperatures. From the literature and our own experience, we know that it is important to show reversibility and to approach equilibrium. Therefore, after mixing the two gas components, we cooled the samples over a period of days. We took Raman scattering spectra of samples with perfect optical quality. From the reproducibility of data, such as $\omega(T, x)$ during cooling and heating cycles, we could deduce that our samples were in equilibrium (metastable or stable). We were able to determine the true concentrations of mixtures from the Raman vibron band intensities via the Raman cross-sections in liquid phase, which deviated substantially from the concentrations found from partial gas pressures. Using characteristics of optical spectra as fingerprints, we were able to assign phase transitions. We derived a $T-x$ phase diagram from our optical spectra and compared this diagram with those reported in the literature on the basis of structural analysis. Since we studied samples in the thermodynamic equilibrium we could answer some open questions and settle discrepancies known in the literature. From Raman band intensities, we determined quantitatively the solubility of O_2 in N_2-based phases.

In addition, we performed high-pressure studies (up to 25 GPa) of this mixture at low temperatures, but only on the N_2-rich side of the binary phase diagram (2% and 7% O_2 in N_2). Comparing the Raman spectra in the vibrational and phonon regions of this mixture to those of pure N_2 we were able to identify phase transitions and to establish a preliminary $p-T-x$ phase diagram. We found that 2% and 7% O_2 is soluble in ϵ*-N_2 (2 GPa $< p <$ 15 GPa), whereas $<$ 1% O_2 can be dissolved in N_2 at ambient pressure. Above 15 GPa in the mixture with 7% O_2 we registered additional spectral features which must be assigned to ϵ*-O_2. This means that O_2 is demixed from ϵ*-N_2 to form ϵ*-O_2 above a certain pressure. The ϵ*-phase of oxygen with an amount N_2 molecules dissolved in it explains the features of the formerly called "new phase". We checked this assumption by a quick control experiment on the O_2-rich side of this mixture. The analysis of band frequencies as a function of pressure at different concentrations enabled us to determine the environmental shift of oxygen molecules in the mixture which is a result of the intermolecular potential $U(N_2-O_2)$ between different types of molecules.

Acknowledgment. We appreciate the help of A. Nickolaus, C. Groeger, and K. Damde in the early stage of these studies, and we thank A. Brodyanski for stimulating discussion. We are also grateful to B. Eckert for the critical examination of the manuscript. One of us (H.-J. J.) thanks INFM for financial support during a research stay at LENS, Florence.

References and Notes

(1) Andrews, L. *Chemistry and Physics of Matrix-isolated Species*; North-Holland: Amsterdam, 1989; Barnes, A. J.; Hallam, H. E. In *Vibrational Spectroscopy—Modern Trends*; Barnes, A. J, Orville-Thomas, W. J., Eds.; Elsevier: Amsterdam, 1977.

(2) Quirico, E.; Schmitt, B. *Icarus* **1997**, *128*, 181.
(3) Nosé, S.; Klein, M. L. *Mol. Phys.* **1983**, *50*, 1055; *Can. J. Phys.* **1982**, *60*, 1365; Schettino, V.; Califano, S. J. *Mol. Struct.* **1983**, *100*, 459.
(4) Hemley, R. J. *Annu. Rev. Phys. Chem.* **2000**, *51*, 763.
(5) Klein, M. L.; Venables, J. A. *Rare Gas Solids*; Academic Press: London, 1977; van Kranendonk, J. *Solid Hydrogen*; Plenum Press: New York, 1983.
(6) Rich, N. H.; Clouter, M. J.; Kiefte, H.; Ahmad, S. F. *Can. J. Phys.* **1982**, *60*, 1358.
(7) Däufer, H.; Löwen, W.; Jodl, H.-J. *J. Mol. Struct.* **1988**, *174*, 11.
(8) De Kinder, J.; Bouwen, A.; Goovaerts, E.; Shoemaker, D. J. *Chem. Phys.* **1990**, *95*, 2269; De Kinder, J.; Goovaerts, E.; Bouwen, A.; Schoemaker, D. *Phys. Rev. B* **1991**, *44*, 10369.
(9) Westerhoff, T.; Feile, R. *Phys. Rev. B* **1993**, *54*, 913; **1996**, *100*, 417.
(10) Lotz, H. T.; Schouten, J. A. *Phys. Rev. B* **2001**, *64*, 024103 and references therein.
(11) Klee, H.; Knorr, K. *Phys. Rev. B* **1991**, *43*, 8658; Jin, L.; Knorr, K. *Phys. Rev. B* **1993**, *47*, 14142.
(12) Manzhelii, V. G.; Prokhvatilov, A. I.; Minchina, I. Ya.; Yantsevich, L. D. *Handbook of Binary Solutions of Cryocrystals*; Begell House: New York, 1996.
(13) Ruheman, M.; Lichter, H.; Komarov, P. *Phys. Z. Sovjetunion* **1935**, *8*, 326.
(14) Barrett, C. S.; Meyer, L.; Greer, S. C.; Wasserman, J. *J. Chem. Phys.* **1968**, *48*, 2670.
(15) Baryl'nik, A. S.; Prokhvatilov, A. I.; Yantsevich, L. D. *Sov. J. Low Temp. Phys.* **1989**, *15*, 282.
(16) Pritula, I. M.; Khashchina, L. V. *Sov. J. Low Temp. Phys.* **1992**, *18* (9), 727.
(17) Freiman, Yu. A.; Tretyak, S. M.; Jezowski, A. *Low Temp. Phys.* **2000**, *26*, 1029.
(18) Baer, B. J.; Nicol, M. *J. Phys. Chem.* **1989**, *93*, 1683; Baer, B. J.; Nicol, M. *J. Phys. Chem.* **1990**, *94*, 1073.
(19) Damde, K.; Jodl, H.-J. *J. Low Temp. Phys.* **1998**, *111*, 327.
(20) Minenko, M.; Jodl, H.-J. To be published.
(21) Hirsch, K. R.; Holzapfel, W. B. *Rev. Sci. Instrum.* **1981**, 52 (1), 52.
(22) Weber, A. *Raman Spectroscopy of Gases and Liquids*; Springer-Verlag: Berlin, 1979.
(23) Bender, E. *The Calculation of Phase Equilibra from a Thermal Equation of State Applied to the Pure Fluids Argon, Nitrogen, Oxygen and their Mixtures*; Verlag C. F. Müller: Karlsruhe, 1973.
(24) Scott, T. A. *Solid and Liquid Nitrogen*; Physics Reports **1976**, *27*, 89.
(25) Freiman, Yu. A.; Jodl, H.-J. *Low Temp. Phys.* **2002**, *28*, 691.
(26) Kreutz, J.; Jodl, H.-J. *Phys. Rev. B* **2003**, *68*, 214303.
(27) Molter, M. Diploma thesis, University of Kaiserslautern, 1984.
(28) Herzberg, G. *Molecular spectra and molecular structure I. Spectra of diatomic molecules*; Van Nostrand Reinold: New York, 1950.
(29) Buckingham, A. D. *Proc. R. Soc. London* **1958**, Ser. A 248, 169; *Faraday Soc. Trans.* **1960**, 56, 26.
(30) Beck, R.; Nibler, J. W. *Chem. Phys. Lett.* **1989**, *159*, 79; Beck, R. D.; Hineman, M. F.; Nibler, J. W. *J. Chem. Phys.* **1990**, *92*, 7068.
(31) Brodyanski, A. P.; Medvedev, S. A.; Vetter, M.; Kreutz, J.; Jodl, H.-J. *Phys. Rev. B* **2002**, *66*, 104301.
(32) Bader, R. F. W.; Henneker, W. H.; Cade, P. E. *J. Chem. Phys.* **1967**, *46*, 3341.
(33) Cahill, J. E.; Leroi, G. E. *J. Chem. Phys.* **1969**, *51*, 97 and 1324.
(34) Bini, R.; Ulivi, L.; Kreutz, J.; Jodl, H. J. *J. Chem. Phys.* **2000**, *112*, 8522.
(35) Cromer, D. T.; Mills, R. L.; Schiferl, D.; Schwalbe, L. A. *Acta Crystallogr.* **1981**, B37, 8; Mills, R. L.; Olinger, B.; Cromer, D. T. *J. Chem. Phys.* **1986**, *84*, 2837.
(36) Jodl, H. J.; Bolduan, F.; Hochheimer, K. D. *Phys. Rev. B* **1985**, *31*, 7376.
(37) Hellwig, H.; Daniels, W. B.; Hemley, R. J.; Mao, H.; Gregoryanz, E. *J. Chem. Phys.* **2001**, *115*, 10876.
(38) Weck, G.; Loubeyre, P.; LeToullec, R. *Phys. Rev. Lett.* **2002**, *88*, 035504; Gorelli, F. A.; Ulivi, L.; Santoro, M.; Bini, R. *Phys. Rev. B* **2001**, *63*, 104110.
(39) Syassen, K.; Nicol, M. In *Physics of Solids under High Pressure*; Schilling, J. S.; Shelton, R. N., Eds.; North-Holland: Amsterdam, 1981.
(40) See Textbooks; for application to spectroscopy, see, e.g., Jodl, H.-J.; Theysohn, G.; Bruno, R. *Phys. Status Solidi B* **1979**, *94*, 161; Nosé, S.; Klein, M. L. *Can. J. Phys.* **1982**, *60*, 1365; Kooi, M. E.; Michels, J. P.; Schouten, J. A. *J. Chem. Phys.* **1999**, *110*, 3023.
(41) Zumofen, G.; Dressler, K. *J. Chem. Phys.* **1976**, *64*, 5198; Zumofen, G. *J. Chem. Phys.* **1978**, *68*, 3747; Thiery, M. M.; Chandrasekharan, V. *J. Chem. Phys.* **1977**, *67*, 3659.
(42) Behringer, R. E. *J. Chem. Phys.* **1958**, *29*, 537.
(43) Schneider, H.; Häfner, W.; Wokaun, A.; Olijnyk, H. *J. Chem. Phys.* **1992**, *96*, 8046.